Int J Fract (2007) 146:105–121
DOI 10.1007/s10704-007-9151-9

ORIGINAL PAPER

Effects of loading rate, notch geometry and loading mode on the local cleavage fracture stress of a C–Mn steel

G. Z. Wang · Y. L. Wang

Received: 17 July 2007 / Accepted: 12 October 2007 / Published online: 31 October 2007

Abstract In this work, notched specimens with two notch geometries were tested in two loading modes (four-point bending (4PB) and three-point bending (3PB)) at various loading rates at a temperature of −110°C for a C–Mn steel. An elastic–plastic finite-element method (FEM) is used to determine the stress distributions ahead of notches. By accurately measuring the distances of the cleavage initiation sites from the notch roots, the local cleavage fracture stress σ_f is measured. The results obtained and combining with previous studies by the authors show that the local cleavage fracture stress σ_f is closely related to the cleavage fracture mechanism (critical events) in steels. The σ_f values do not change with loading rate, notch geometry and loading mode, as long as the critical event of cleavage fracture does not change at various testing conditions. The σ_f is mainly determined by the steel microstructure, and its scatter is mainly caused by the size distribution of the weakest constituent in steels (ferrite grain or pearlite colony with large sizes and large second phase particles) and the change of the critical events in cleavage process. The σ_f can characterize the intrinsic toughness of steels and may be used in a "local approach" model for assessing integrity of flawed structures. The σ_f values could be measured by both 4PB and 3PB tests.

Keywords Local cleavage fracture stress · Loading rate · Notch geometry · Loading mode · FEM · C–Mn steel

G. Z. Wang (✉)
School of Mechanical and Power Engineering, East China University of Science and Technology, Shanghai 200237, China
e-mail: wanggz1965@163.com

Y. L. Wang
State Key Laboratory of Advanced Non-Ferrous Metal Materials, Lanzhou University of Technology, Lanzhou 730050, China

1 Introduction

It is well known that the cleavage fracture of ferrite steels is controlled by a critical local tensile stress criterion ($\sigma_{yy} \geq \sigma_f$) (Knott 1966; Tetelman et al. 1968; Ritchie et al. 1973; Thompson and Knott 1993). A salient feature of cleavage fracture is the variability of experimental results. An extensive scatter band of measured values is usually observed for global parameters assessing fracture toughness such as K_{1c}, J_{1c} and COD. A lot of probabilistic models have been developed to describe the distribution of the measured scatter (Beremin 1983; Wallin 1984; Lin et al. 1986; Mudry 1987; Minami et al. 1992; Ruggieeri and Dodds 1996; Gao et al. 2001). Most models are based on the weakest link theory, i.e., the whole specimen fails at the moment when the normal stress σ_{yy} exceeds the local fracture stress σ_f and propagates a cleavage crack in a carbide particle. A Weibull probability function of the normal stress is used to a large extent to describe the scatter of measured fracture toughness values. Therefore, σ_f is an important parameter for the cleavage fracture models.

These Weibull stress models (Beremin 1983; Wallin 1984; Lin et al. 1986; Mudry 1987; Minami et al. 1992; Ruggieeri and Dodds 1996; Gao et al. 2001) employ only two or three parameters (Weibull shape factor m, scale parameter σu and threshold stress σth) to describe the cleavage event, and the potential dependencies of these Weibull parameters on temperature, loading rate, irradiation, pre-straining, specimen geometry, etc., remain largely open issues (Mudry 1987; Gao et al. 2001).

The local cleavage fracture stress σ_f is regarded as a decisive factor controlling cleavage fracture and toughness of various steels (Ritchie et al. 1976, 1979; Curry 1980; Ritchie and Thompson 1985; Lin et al. 1986; Kavishe and Baker 1986; Lewandowski and Thompson 1986; Samant and Lewandowski 1997). It is related to the Weibull stress parameters in the Weibull stress model mentioned above. The Weibull stress model is the base for the development of a "local approach" for the assessment of the mechanical integrity of any flawed mechanical structure, and it needs to be corrected based on the actual cleavage fracture mechanism and physical model of steels (Pineau 2006). Therefore, for developing realistic physical and probabilistic models of cleavage fracture, the factors influencing the local cleavage fracture stress σ_f should be investigated.

The early works (Chen et al. 1990a, 1997a; Wang et al. 2001) have shown that the σ_f was nearly independent of test temperature. However, the effects of loading rate, notch geometry and loading mode on the σ_f have not been completely validated. In previous works (Chen et al. 1990a, b), σ_f values estimated from Charpy V impact test are essentially the same as that measured by four-point bending (4PB) specimens tested at quasi-static loading, thus it is considered that the σ_f is nearly independent of loading rate. In recent studies by the authors (Wang et al. 2004a, 2005), 4PB tests of notched specimens loaded at various loading rates for low alloy steels with different grain sizes and a C–Mn steel were done, and the finite-element method (FEM) calculations were carried out. It was found that the measured σ_f values do not change with loading rate, as long as the critical event of cleavage fracture does not change. The steel with fine ferrite grains have higher σ_f values and notch toughness, and its critical event of cleavage fracture is the propagation of a ferrite grain-sized crack.

About the effects of the notch geometry on the σ_f, (Tetelman et al. 1968) investigated the effect of notch root radius on the local cleavage fracture stress σ_f by means of slip-line field analysis. They suggested that when the root radius was larger than 0.254 mm, σ_f may vary with root radius, because of differences in stressed volumes. The work of Lewandowski and Thompson (1986) shows that the σ_f of fully pearlitic microstructure was independent of notch root radius. Yan et al. (1993) evaluated the effect of the notch root radius on σ_f by using FEM analysis and 4PB tests for fine-grain and coarse-grain C–Mn steel. For both fine grains and coarse grains, when the notch root radius increased from 0.25 mm to 1 mm, the stressed volume and fracture load showed marked variations, but σ_f remained relatively constant. Cleavage fracture was related to the elevation of normal stress ahead of the notch and σ_f was independent of the notch root radius. One of the authors (Wang et al. 1999) of this paper investigated the effect of notch depth and notch flank angle on σ_f using FEM analysis and 4PB tests. With increasing notch depths and notch flank angle, the fracture load and "high stress volume" showed marked variation, but σ_f remained relatively constant. The cleavage fracture was related to the elevation of normal stress ahead of the notch and was controlled by the criterion $\sigma_{yy} \geq \sigma_f$. The critical event for cleavage fracture is the propagation of a ferrite grain-sized crack into the neighboring matrix and was independent of the notch depth and flank angle. σ_f was determined by ferrite grain size with a statistical variation.

The study about effect of loading mode on the σ_f can not almost be found in literature. The local cleavage fracture stress σ_f was commonly measured by loading notched specimens in 4PB mode (Ritchie et al. 1973, Lewandowski and Thompson 1986; Samant and Lewandowski 1997; Wang et al. 1999, 2003). The effects of other loading modes on the σ_f, such as three-point bending (3PB) and mixed mode I/II loading, have not been clarified.

In this work, notched specimens with two notch geometries were tested in two loading modes (4PB and 3PB) at various loading rates at a temperature of −110°C for a C–Mn steel. An elastic-plastic FEM is used to determine the stress distributions ahead of notches. By accurately measuring the distances of the cleavage initiation sites from the notch roots, the local cleavage fracture stress σ_f is measured. Based on the results obtained and combining with previous studies (Wang et al. 1999, 2001, 2003, 2004a, b, 2005) by the authors, the effects of loading rate, notch geometry and loading mode on the σ_f are further fully investigated.

2 Experimental procedures

2.1 Materials, specimens and experiments

A C–Mn vessel steel is used. The composition (mass%) of the steel is C = 0.18, Mn = 1.49, Si = 0.36, S = 0.03, and P = 0.01, and the microstructure is composed of ferrite and pearlite.

Tensile, 4PB and 3PB specimens are shown in Fig. 1. The 4PB and 3PB specimens with same dimensions were cut in the L–T orientation. It means that the notch plane is parallel to L direction (longitudinal direction of the steel plate) and vertical to T direction (transverse direction of the steel plate). The dimensions of the 4PB specimens (4V and 4I) (Fig. 1b) and the 3PB specimens (3V and 3I) (Fig. 1d) with two notch geometries are listed in Table 1. The 4V/3V and 4I/3I specimens have the same thickness $W=$ 12.7 mm, width $B = 12.7$ mm and notch depth $a = 4.25$ mm, but different notch flank angle θ and notch root radius ρ. The notch flank angle and notch root radius of the 4V and 3V specimens ($\theta = 90°$, $\rho = 0.25$ mm) are larger than that of the 4I and 3I specimens ($\theta = 0°$, $\rho = 0.14$ mm). The double notch 4PB specimens (Fig. 1c) are used for observing the remaining micro cracks.

Tensile specimens were tested at various loading rates at a temperature of −110°C. The true stress σ of the steel as function of plastic strain ε_p ($\sigma - \varepsilon_p$ curves) for different strain rates was measured. The 4PB and 3PB tests were carried out at different loading rates of 1, 60, 120, 240, 360 and 500 mm/min by a universal test machine SHIMADZU AG-10T at −110°C (to ensure the fracture mode of the steel is cleavage), and the curves of the load and load-line displacement were recorded automatically. The fracture load P_f was measured by the load–displacement curve.

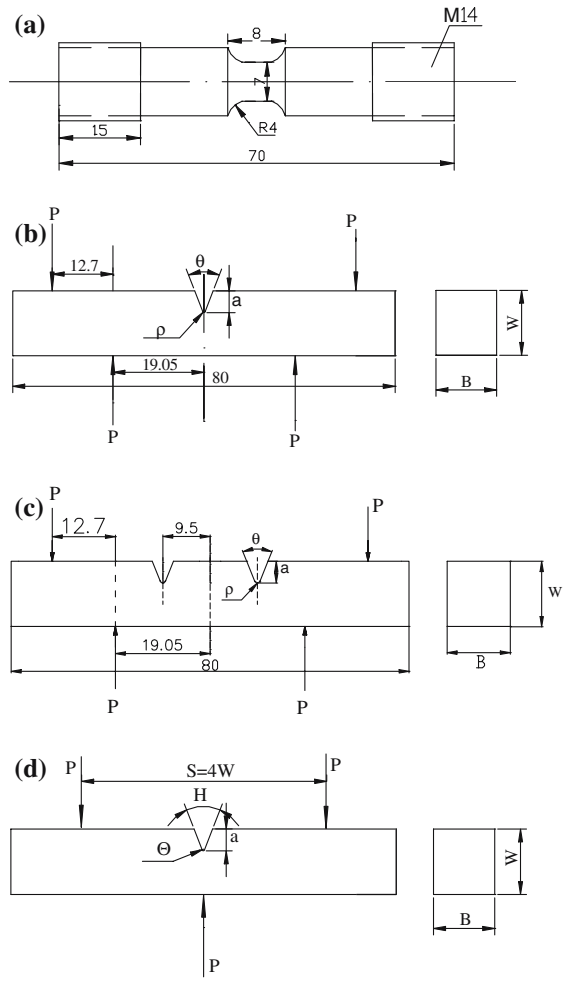

Fig. 1 Tensile and four-point bending (4PB) specimens: (**a**) tensile specimen, (**b**) single notch 4PB, (**c**) double notches 4PB, (**d**) three-point bending (3PB) (The unit is mm)

2.2 Microscopic observation

Fracture surfaces of all specimens were observed in detail with a scanning electron microscope Hitachi

Table 1 The dimensions of the 4PB specimens

Specimen	W (mm)	B (mm)	a (mm)	a/w	ρ (mm)	θ (°)
4V	12.7	12.7	4.25	0.335	0.25	90
4I	12.7	12.7	4.25	0.335	0.14	0
3V	12.7	12.7	4.25	0.335	0.25	90
3I	12.7	12.7	4.25	0.335	0.14	0

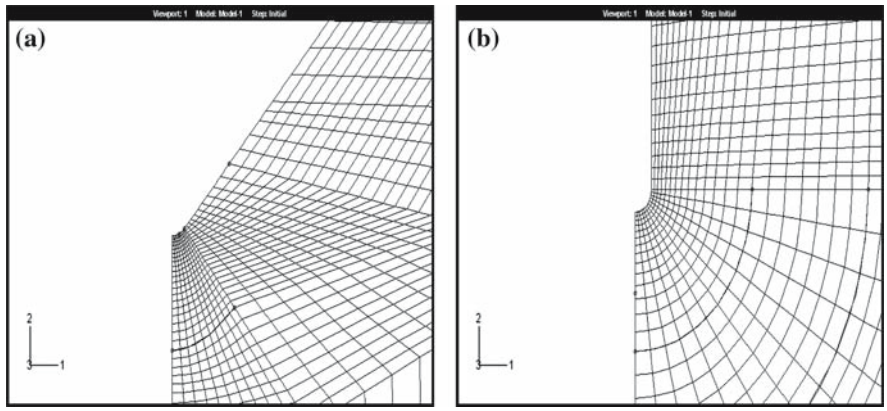

Fig. 2 Element arrangement in the vicinity of the notch root for the two notch geometries: (**a**) 4V specimen, (**b**) 4I specimen

Table 2 Parameters in FEM models

Specimen	Number of elements	Number of nodes	Minimum element sizes (μm)
3V	2950	3094	20.1
3I	3076	3222	18.3
4V	3140	3286	20.1
4I	3150	3298	18.3

S-520 (Japan). The initiation site of cleavage fracture was located by tracing the river pattern strips back to their origin with the similar method used by previous researches (Wang et al. 2003; Chen et al. 1991, 1996; Chen and Yan 1992). The distance of the cleavage initiation site from the tip of the blunted notch was measured as X_f. For specimens with fibrous cracking (ductile failure of the material) prior to cleavage the length of the fibrous crack was measured. For doubly notched specimens, fracture occurred at one notch and the critical condition was reached in the vicinity of the survived notch. Six metallographic sections perpendicular to the notch that survived were cut, and were grouped together in a single bakelite mount and polished using standard metallographic techniques. The metallographic sections were etched with 2% Nital to observe the remaining crack and identify the critical event of cleavage using the SEM (Wang et al. 1999, 2003).

2.3 Finite-element method calculation

The maximum normal stress σ_{yy} on the plane directly ahead of the notches and effective plastic strain ε_p ahead of notches were calculated at applied loads from elastic regime to over general yield for the 4PB (4V and 4I) and 3PB (3V and 3I) specimens tested at various loading rates at −110°C. A two dimensional model with four-nodes bilinear plane strain reduced integration elements (CPE4R) was used with the ABAQUS/Explicit procedure in ABAQUS code. Due to symmetry, only one half of the geometry needs to be analyzed. The element arrangement in the vicinity of the notch root for the two notch geometries is shown in Fig. 2. The numbers of elements and nodes and minimum element sizes at the notch tips for all specimens are listed in Table 2. The true stress–plastic strain curves ($\sigma - \varepsilon_p$ curves) at various strain rates obtained from the tensile test results (Fig. 3) were digitized and fit into the series of data for the input file of the FEM code. The various strain rates from the tensile tests were automatically used in different locations ahead of the notch by the FEM code in the FEM simulations. The general yield P_{gy} was calculated by the applied load at which a plastic 'hinge' spreads across the notched cross-section to leave an elastic enclave located on the symmetry axis (Alexander et al. 1986).

2.4 Measurement of the local cleavage fracture stress σ_f

At a measured fracture load P_f, corresponding curves of tensile stress σ_{yy} can be selected from the FEM

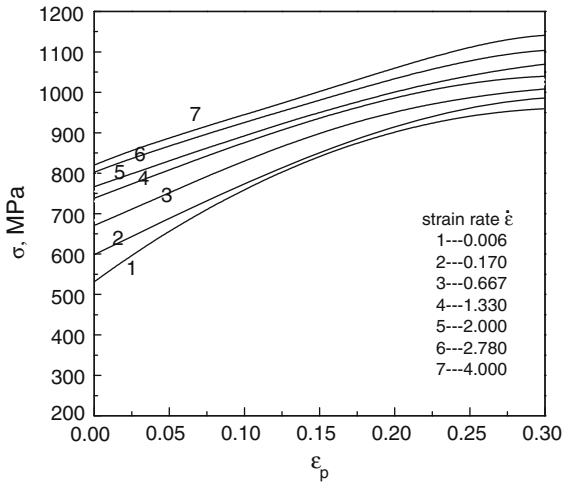

Fig. 3 The true stress σ–plastic strain ε_p curves of the steel at different strain rates

calculation results. With the measured X_f (the distance of the cleavage initiation site from the tip of the blunted notch) as the abscissa, the corresponding ordinate value of the normal stress σ_{yy} of the stress distribution curve (Figs. 4 and 5) was taken as the local cleavage fracture stress σ_f.

3 Results

3.1 Results of tensile tests

Tensile tests were carried out at various loading rates at a temperature of −110°C. The measured true stress σ–plastic strain ε_p curves of the steel at different strain rates are shown in Fig. 3. The stress σ increases with plastic strain ε_p and strain rate $\dot{\varepsilon}$.

3.2 FEM calculation results of stress distributions for the 4PB and 3PB specimens

Typical results of the finite element calculations of the maximum normal stress σ_{yy} distributions on the plane directly ahead of the notches for the 4V/4I and 3V/3I specimens with a loading rate of 240 mm/min are shown in Figs. 4 and 5, where P is the applied load, X is the distance to notch root. In these figures, with increasing load ratio (P/P_{gy}) the normal stress σ_{yy} increases, and the peak of the σ_{yy} moves away from the notch root, resulting in the extension of the areas

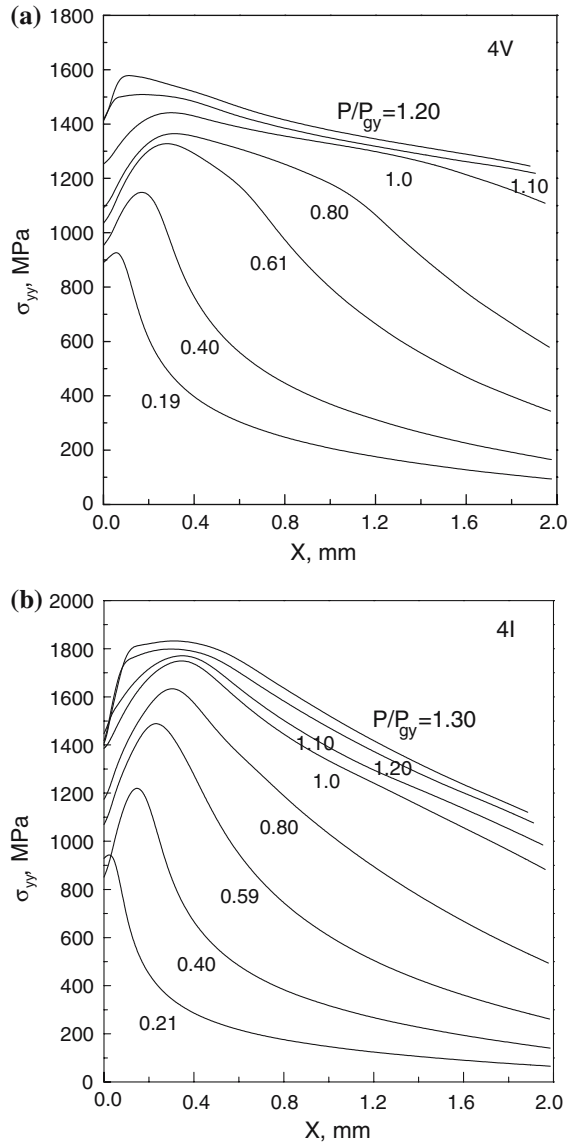

Fig. 4 Distributions of the maximum normal stress σ_{yy} in front of notches calculated by FEM for the 4V (**a**) and 4I (**b**) specimens with a loading rate of 240 mm/min

under high σ_{yy}. This result is similar to the Griffiths-Owen's result (Griffith and Owen 1971). Figures 6 and 7 show the variations of the peak stress σ_{yymax} ahead of notches with applied load ratio P/P_{gy} for the 4V/4I and 3V/3I specimens with various loading rates. The σ_{yymax} increases with increasing P/P_{gy} and it increases rapidly with the P/P_{gy} at $P/P_{gy} < 0.6$, and after that ($P/P_{gy} > 0.6$) it increases slowly. With increasing loading rate V the σ_{yymax} increases. The σ_{yymax} ahead of

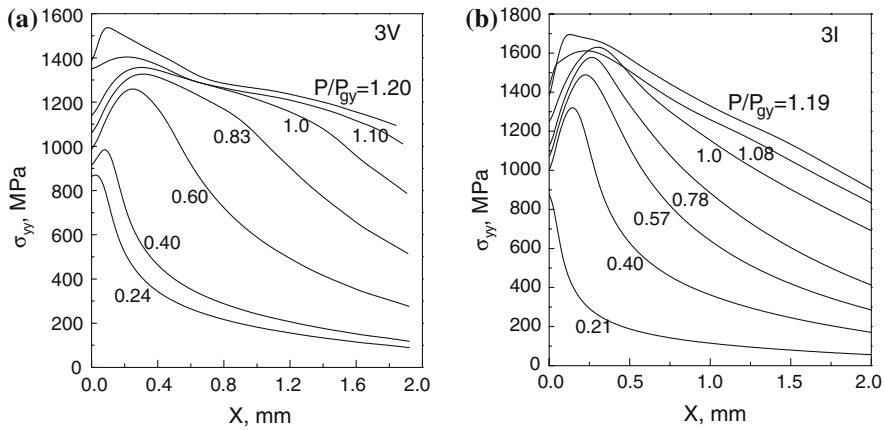

Fig. 5 Distributions of the maximum normal stress σ_{yy} in front of notches calculated by FEM for the 3V (**a**) and 3I (**b**) specimens with a loading rate of 240 mm/min

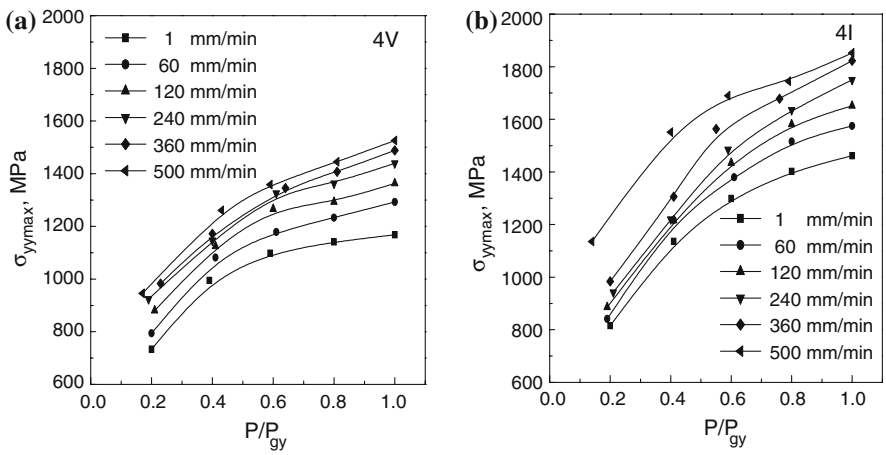

Fig. 6 The variation of the peak stress $\sigma_{yy\,max}$ ahead of notches with applied load ratio P/P_{gy} for the 4V (**a**) and 4I (**b**) specimens with various loading rates

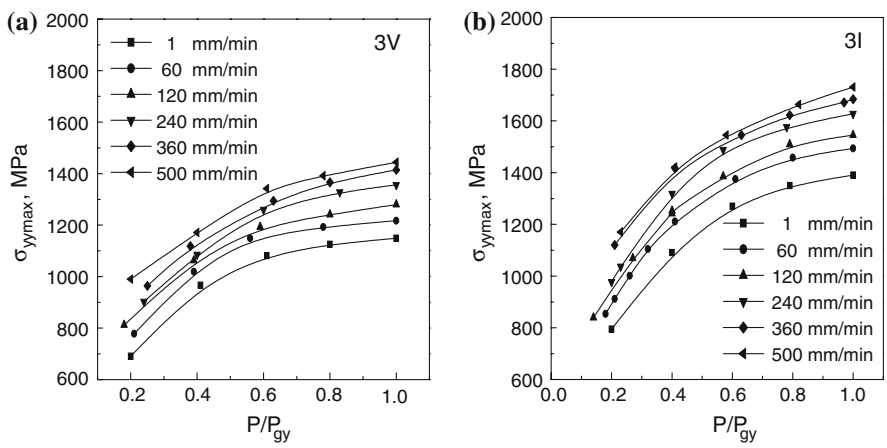

Fig. 7 The variation of the peak stress $\sigma_{yy\,max}$ ahead of notches with applied load ratio P/P_{gy} for the 3V (**a**) and 3I (**b**) specimens with various loading rates

notches of the 4V/3V specimens is lower than that of the 4I/3I specimens, and the σ_{yymax} of the 4V/4I specimens is slightly higher than that of the 3V/3I specimens.

3.3 Results of 4PB and 3PB tests

3.3.1 Results of microscopic observation for 4PB tests

The parameters measured from the 4PB tests for the 4V and 4I specimens are summarized in Tables 3 and 4, respectively. The following ideas are summarized from experimental observations and the data of Tables 3 and 4:

For the 4V specimens in Table 3, in the two specimens with lowest loading rate of 1 mm/min (4V13, 4V04), some short fibrous cracks (their average lengths, Fib, are listed in Table 3) emanating from the notch occur before cleavage initiation, and the cleavage is initiated at a distance from the fibrous crack tip ahead of the notch root. The local cleavage fracture stress could not be measured in these specimens due to the ductile tearing at the notch tips. For all the 4V specimens with loading rates larger than 1 mm/min, the fracture mode is cleavage. In some specimens with various loading rates, the distance X_f from the cleavage-initiating site to the notch root is zero. In this case the cleavages are directly initiated at the notch tips, as typically shown in Fig. 8. In the other specimens the values of X_f are in a range of 96–1269 μm. This means that the cleavages are initiated at various distances ahead of notch root at various loading rates, as typically shown in Fig. 9. On the metallographic sections of doubly notched specimens with various loading rates, the remaining cracks that mainly limited in ferrite grains with a length of 10–40 μm were found, which is located in a range of X = 0–80 μm close to notch roots. The most cracks are located at notch tips (X = 0), and some of them is blunted, as typically shown in Fig. 10. In the range

Table 3 4PB test results for the 4V specimens

No.	V (mm/min)	P_f (KN)	P_f/P_{gy}	X_f (μm)	σ_f (MPa)	Fib (μm)
4V13	1	41.16	1.39	891	–	470
4V04	1	43.86	1.49	170	–	98
Ave	1	42.51	1.44	531	–	284
4V18	60	32.59	1.03	96	1313	0
4V05	60	42.88	1.35	982	1312	0
4V30	60	32.34	1.02	0	1232	0
Ave	60	35.93	1.13	359	1286	0
4V11	120	35.28	1.07	476	1387	0
4V26	120	32.24	0.98	717	1291	0
Ave	120	33.76	1.03	597	1339	0
4V28	240	33.57	0.98	0	1221	0
4V03	240	32.93	0.96	1269	1244	0
4V21	240	34.89	1.01	0	1284	0
Ave	240	33.79	0.98	423	1250	0
4V19	360	29.79	0.84	0	1134	0
4V02	360	34.59	0.98	0	1233	0
Ave	360	32.19	0.91	0	1184	0
4V09	500	35.28	0.97	368	1505	0
4V07	500	33.61	0.93	0	1241	0
4V29	500	26.85	0.74	0	1141	0
Ave	500	31.92	0.88	123	1296	0

No.: specimen number; V: loading rate; P_f: fracture load; P_{gy}: general yield load; X_f: distance from cleavage origin to notch tip; σ_f: local cleavage facture stress; Fib: length of fibrous crack

Table 4 4PB test results for the 4I specimens

No.	V (mm/min)	P_f (KN)	P_f/P_{gy}	X_f (μm)	σ_f (MPa)	Fib (μm)
4I24	1	32.10	1.06	853	–	94
4I17	1	27.24	0.90	298	1390	0
4I30	1	25.48	0.84	0	978	0
Ave	1	28.27	0.93	384	1184	31.3
4I08	60	24.75	0.76	404	1451	0
4I25	60	25.58	0.79	391	1484	0
Ave	60	25.16	0.78	398	1468	0
4I31	120	17.64	0.52	0	1052	0
4I27	120	13.62	0.40	0	984	0
4I05	120	26.17	0.77	0	1110	0
Ave	120	19.14	0.56	0	1049	0
4I09	240	21.07	0.59	330	1384	0
4I26	240	21.95	0.61	195	1512	0
Ave	240	21.51	0.60	263	1448	0
4I21	360	22.25	0.60	447	1102	0
4I28	360	10.49	0.28	0	1089	0
4I10	360	24.30	0.66	326	1690	0
Ave	360	19.01	0.51	258	1294	0
4I12	500	10.49	0.28	0	1081	0
4I29	500	11.66	0.31	0	1097	0
Ave	500	11.07	0.30	0	1089	0

No.: specimen number; V: loading rate; P_f: fracture load; P_{gy}: general yield load; X_f: distance from cleavage origin to notch tip; σ_f: local cleavage facture stress; Fib: length of fibrous crack

larger than 80 μm away from the notch root, no remaining cracks were found.

For the 4I specimens (in Table 3), in one specimen with loading rate of 1 mm/min (4I24), short fibrous cracks (its average length, Fib, are listed in Table 3) emanating from the notch root also occur before cleavage initiation. For all other specimens with various loading rates, the fracture mode is cleavage, and the cleavage initiation behavior is similar to the 4V specimens. In some specimens with various loading rates, the cleavages are directly initiated at the notch tips ($X_f = 0$) (similar to Fig. 8). In the other specimens the cleavages are initiated at various distances (X_f = 195–447 μm) ahead of notch roots at various loading rates (similar to Fig. 9). On metallographic sections of doubly notched specimens with various loading rates, the remaining cracks that mainly limited in ferrite grains with a length of 10–40 μm were also found in a range of X = 0–80 μm close to notch roots. And the most cracks are located at notch tips (X = 0), as typically shown in Fig. 11. In the range larger than 80 μm away from notch root, no remaining cracks were found.

3.3.2 Results of microscopic observation for 3PB tests

The parameters measured from the 3PB tests for the 3V and 3I specimens are summarized in Tables 5 and 6, respectively. The results are similar to the 4V and 4I specimens. The following ideas can also be summarized from experimental observations and the data in Tables 5 and 6:

For the 3V specimens in Table 5, in one specimen with the lowest loading rate of 1 mm/min (3V10), short fibrous cracks (its average lengths, Fib, are listed in Table 5) emanating from the notch occur before cleavage initiation, and the cleavage is initiated at a distance from the fibrous crack tip ahead of the notch root. The local cleavage fracture stress could not be measured in this specimen due to the ductile tearing at the notch tip. For all the 3V specimens with loading rates larger than

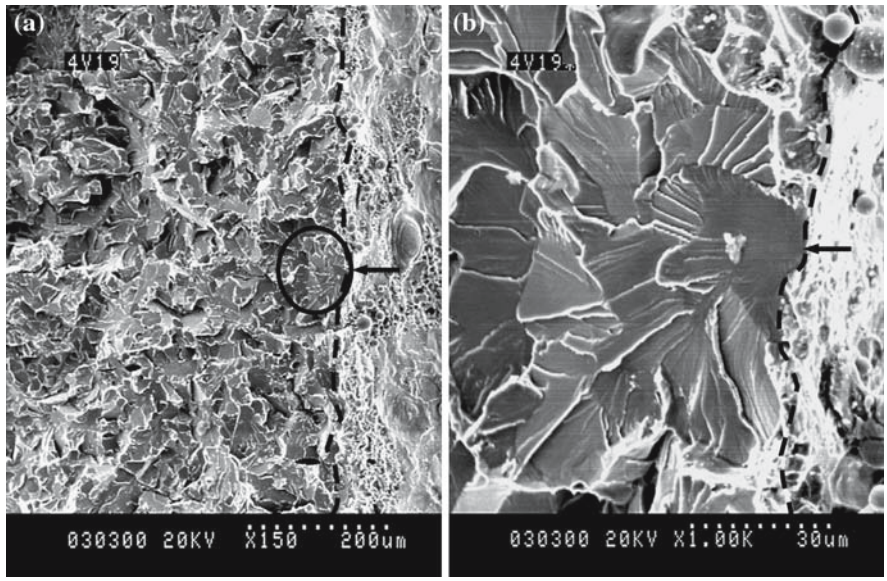

Fig. 8 Typical fracture surface showing cleavage directly initiated at the notch tip by a black arrow (**a**) for a 4Vspecimen at a loading rate of V = 360 mm/min, (**b**) close look

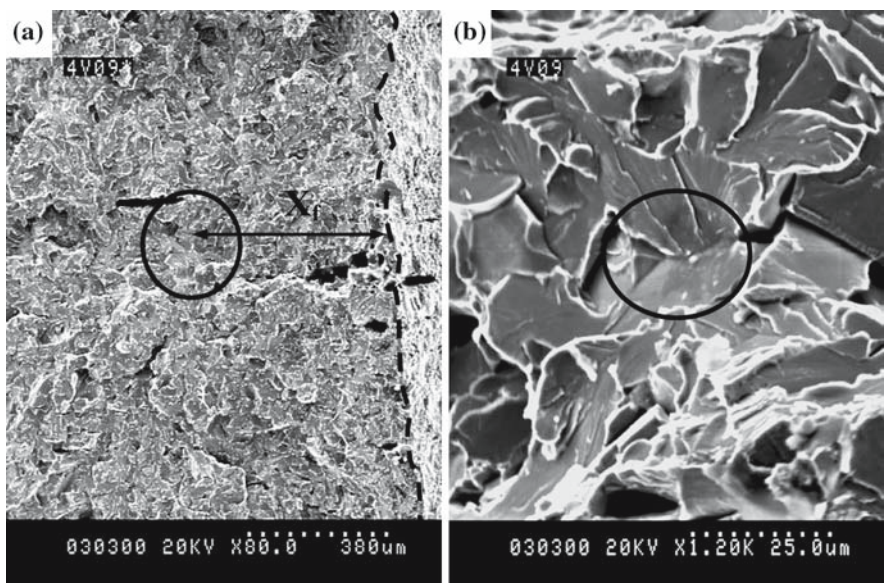

Fig. 9 Typical fracture surface showing cleavage initiated at a distances X_f ahead of notch root (**a**) for a 4V specimen at a loading rate of V = 500 mm/min, (**b**) close look

1 mm/min, the fracture mode is cleavage. In some specimens with various loading rates, the distance X_f from the cleavage-initiating site to the notch root is zero. In this case the cleavages are directly initiated at the notch tips, as typically shown in Fig. 12. In the other specimens the values of X_f are in a range of 170–1380 µm. This means that the cleavages are initiated at various distances ahead of notch root at various loading rates, and it is similar to Figs. 9 and 13.

For the 3I specimens (in Table 6), the fracture mode of all specimens with various loading rates is cleavage, and the cleavage initiation behavior is similar to the 3V specimens. In some specimens with various loading rates, the cleavages are directly initiated at the notch tips ($X_f = 0$) (similar to Fig. 8 and 12). In other specimens the cleavages are initiated at various distances (X_f = 61–652 µm) ahead of notch roots at various loading rates, as typically shown in Fig. 13.

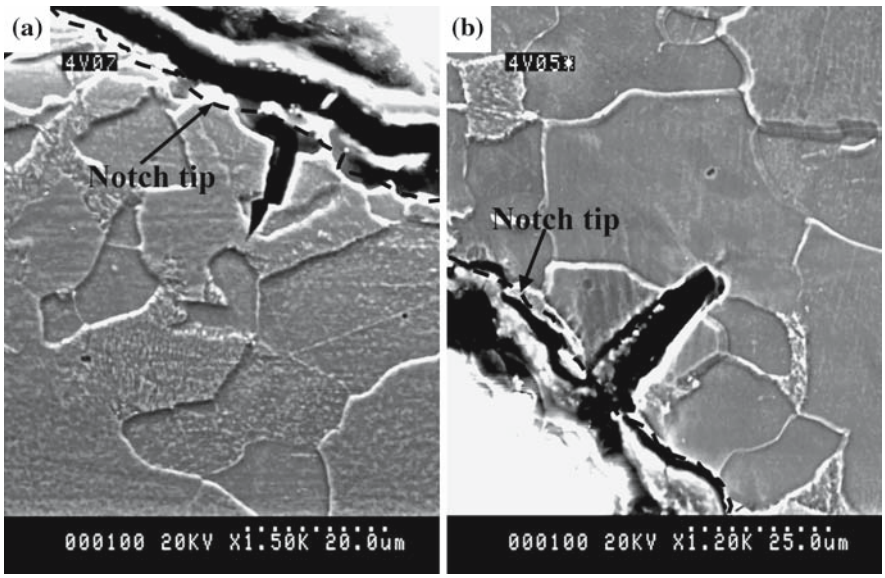

Fig. 10 Typical ferrite grain-sized remaining microscopic cracks found at survived notch tips of the fractured doubly notched specimens for 4 V specimens. (**a**) loading rate V = 500 mm/min, (**b**) V = 60 mm/min

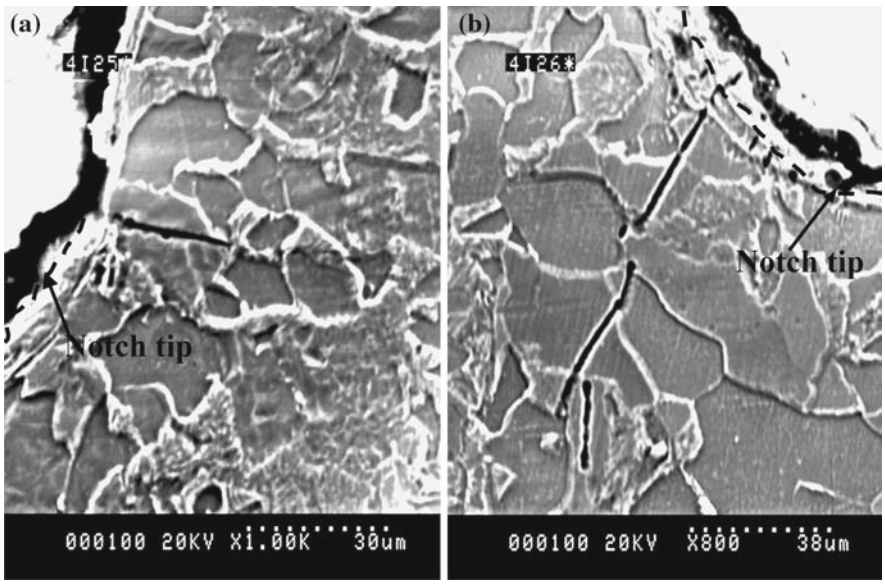

Fig. 11 Typical ferrite grain-sized remaining microscopic cracks found at survived notch tips of the fractured doubly notched specimens for 4I specimens. (**a**) loading rate V = 60 mm/min, (**b**) V = 240 mm/min

3.3.3 Measuring results of the local cleavage fracture stress

The measuring values of the local cleavage fracture stress σ_f for the 4PB and 3PB specimens are listed in Tables 3/4 and 5/6. Figure 14 shows the variation of the σ_f measured in 4V and 4I specimens (Fig. 14a) and in 3V and 3I specimens ((Fig. 14b) with loading rate V. The data marked by the solid symbols are the σ_f values measured in the specimens with $X_f = 0$, and that by the open symbols are the σ_f values in the specimens with $X_f \neq 0$. All σ_f values of the 4V, 4I, 3V and 3I specimens are in the same scatter range of 1000–1500 MPa. This means that the local cleavage fracture stress σ_f does not essentially change with loading rate V, notch geometry and loading mode (4PB and 3PB). The σ_f values corresponding to $X_f = 0$ are lower than that corresponding to $X_f \neq 0$.

Table 5 4PB test results for the 3V specimens

No.	V (mm/min)	P_f (KN)	P_f/P_{gy}	X_f (μm	σ_f (MPa)	Fib (μm)
3V10	1	14.95	1.10	167	–	188
3V23	1	14.70	1.08	104	1179	0
Ave	1	14.82	1.09	134	1179	94
3V17	60	17.15	1.18	292	1326	0
3V12	60	15.93	1.10	1380	1112	0
3V27	60	16.42	1.13	235	1279	0
Ave	60	16.50	1.14	636	1196	0
3V01	120	15.88	1.07	0	1375	0
3V32	120	15.64	1.05	1151	1173	0
3V31	120	15.48	1.04	387	1280	0
Ave	120	15.67	1.05	513	1276	0
3V22	240	15.00	0.98	170	1305	0
3V14	240	15.60	1.02	0	1140	0
Ave	240	15.30	1.0	85	1223	0
3V08	360	12.62	0.81	0	1065	0
3V16	360	16.97	1.09	415	1412	0
3V20	360	15.52	1.0	0	1274	0
Ave	360	15.04	0.97	138	1250	0
3V24	500	16.86	1.07	526	1418	0
3V25	500	16.15	1.03	182	1435	0
3V15	500	15.80	1.0	1212	1208	0
Ave	500	16.27	1.03	640	1354	0

No.: specimen number; V: loading rate; P_f: fracture load; P_{gy}: general yield load; X_f: distance from cleavage origin to notch tip; σ_f: local cleavage facture stress; Fib: length of fibrous crack

4 Discussion

4.1 The critical event of cleavage fracture in the 4PB specimens

The critical event, being the most important link in a process of cleavage, means the most difficult step among the three consecutive steps of a cleavage process; i.e. a crack nucleation in a second-phase particle, the just-nucleated crack passes through the boundary between the second-phase particle and the matrix grain, and the propagation of the grain-sized crack across the grain boundary. The identification of the critical event is very important for developing a realistic physical model of cleavage fracture, understanding the nature of the local cleavage fracture stress and the relationship between toughness and microstructure of various steels. From the late 1960s to 1980s, the critical event of cleavage was considered as the propagation of a second-phase particle-sized crack into the matrix (Curry and Knott 1978; Hahn 1984). However, some works (Mendiratta et al. 1996; Wang and Chen 1998; Wall et al. 1994) found that while the normal tensile stress ahead of a notch root, exceeding the critical local fracture stress, be able to propagate a crack with critical size, the plastic strain is not yet necessarily to have reached a critical value for initiating a crack nucleus. It means that in some cases the crack nucleation still behaves as a critical step for a cleavage process. Therefore for producing cleavage both criteria, a critical plastic strain ($\varepsilon_p \geq \varepsilon_{pc}$) to nucleate a crack and a critical normal stress ($\sigma_{yy} \geq \sigma_f$) to propagate the just nucleated crack should be reached. Thus a dual criterion was suggested (Mendiratta et al. 1996; Wang and Chen 1998).

The characteristic feature of a critical event of crack propagation controlled by tensile stress is that the cracks limited in the microstructural domain that nucleated

Table 6 4PB test results for the 3I specimens

No.	V (mm/min)	P_f (KN)	P_f/P_{gy}	X_f (μm)	σ_f (MPa)	Fib (μm)
3I02	1	13.23	0.89	836	1040	0
3I23	1	11.76	0.79	560	1180	0
Ave	1	12.50	0.84	698	–	0
3I16	60	10.49	0.66	339	1358	0
3I07	60	13.52	0.85	264	1453	0
3I06	60	8.82	0.55	215	1316	0
Ave	60	10.94	0.69	273	1376	0
3I15	120	8.14	0.49	0	974	0
3I19	120	9.70	0.59	0	1013	0
Ave	120	8.92	0.54	6	994	0
3I22	240	10.11	0.59	0	1080	0
3I04	240	8.19	0.48	342	1118	0
Ave	240	9.15	0.54	171	1099	0
3I01	360	10.50	0.60	169	1496	0
3I03	360	7.45	0.42	0	1044	0
3I20	360	13.05	0.74	61	1330	0
Ave	360	10.34	0.59	77	1290	0
3I18	500	7.33	0.41	0	1026	0
3I14	500	14.00	0.78	652	1146	0
3I11	500	9.52	0.53	223	1549	0
Ave	500	10.28	0.57	292	1240	0

No.: specimen number; V: loading rate; P_f: fracture load; P_{gy}: general yield load; X_f: distance from cleavage origin to notch tip; σ_f: local cleavage facture stress; Fib: length of fibrous crack

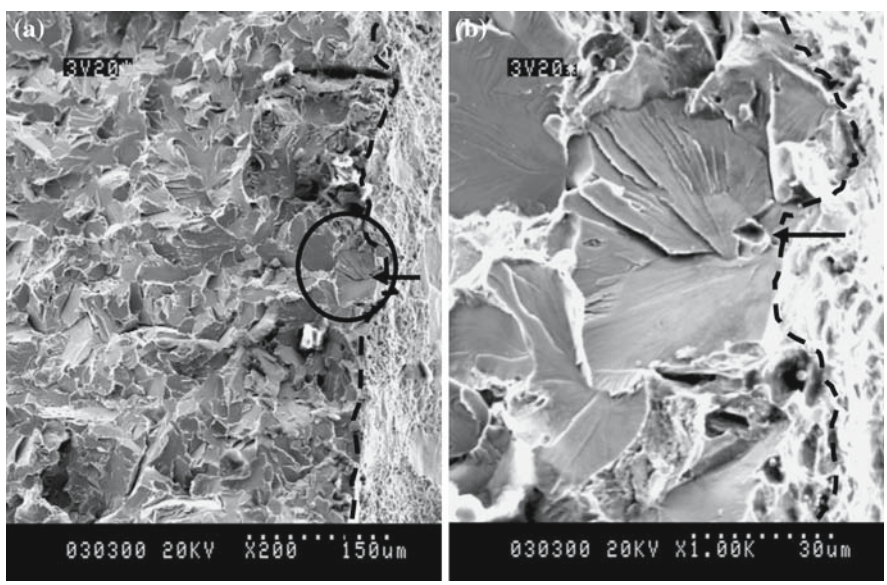

Fig. 12 Typical fracture surface showing cleavage directly initiated at the notch tip by a black arrow (**a**) for a 3 V specimen at a loading rate of V = 360 mm/min, (**b**) close look

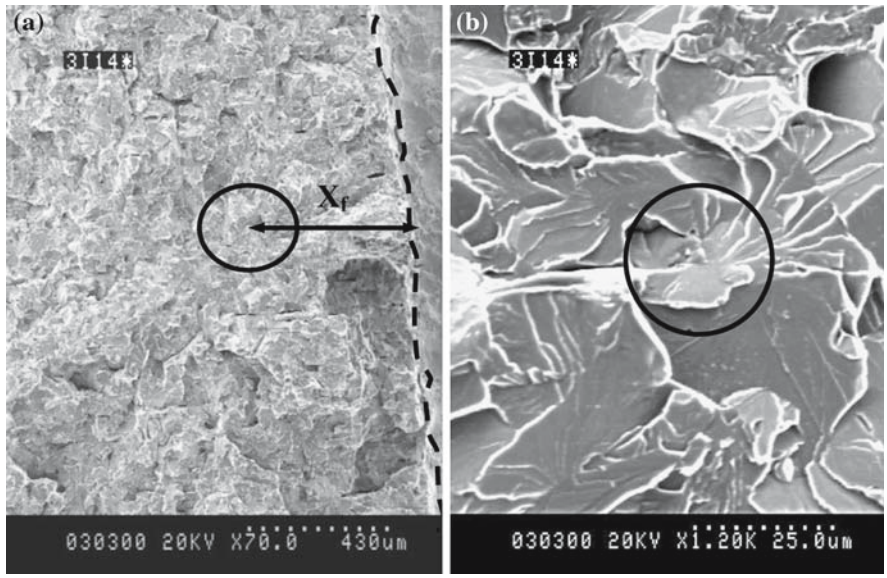

Fig. 13 Typical fracture surface showing cleavage initiated at a distances X_f ahead of notch root (**a**) for a 3I specimen at a loading rate of V = 500 mm/min, (**b**) close look

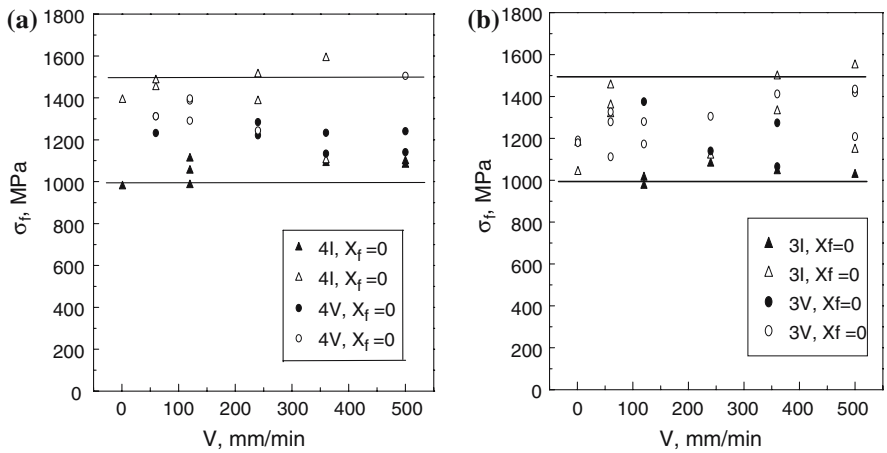

Fig. 14 The local cleavage fracture stress σ_f of the 4V and 4I specimens (**a**) and 3V and 3I specimens (**b**) loaded at various loading rates

but failed to propagate remain in a fractured specimen. Doubly notched specimens are particularly appropriate for observing the remaining cracks in front of the surviving notch after the specimen is fractured at one notch. Because when fracture occurred at one notch, the critical condition was also reached in the vicinity of the survived notch. That a crack remains in front of the surviving notch means the tensile stress was not sufficient to propagate the crack just nucleated. This shows a tensile stress-controlling crack propagation mechanism. However, the characteristic feature of a critical event of crack nucleation is that no remaining crack can be found in the corresponding range of cleavage initiation sites (X_f) ahead of notch root in fractured specimens.

For the steel in this work, the microscopic observations show that for some 4V and 4I specimens tested at various loading rates the cleavages are directly initiated at the notch tips ($X_f = 0$) (Tables 3 and 4, Fig. 8), and many remaining cracks limiting in ferrite grains were also found at notch tips (X = 0) (Figs. 10 and 11). These facts indicate that the critical events in these specimens with $X_f = 0$ are mainly the propagation of a ferrite grain-sized crack controlled by tensile stress. However, for the 4V and 4I specimens with $X_f \neq 0$, the cleavages were initiated in a range of X_f = 96–1269 μm (4V specimens in Table 3) and X_f = 195–447 μm (4I specimens in Table 4), and no remaining cracks were found in the range (the corresponding range of cleavage initiation site X_f) larger than 80 μm away from the survived notch

root of the fractured doubly notched specimen. These facts means that the critical events in these specimens with $X_f \neq 0$ are mainly crack nucleation controlled by plastic strain. Therefore, two cleavage mechanisms corresponding to two critical events of crack propagation and crack nucleation seem to compete in the high stress and strain volume ahead of notch roots at different loading rates tested. From Fig. 14, the lowest cleavage strength of those notch-root constituent (grains and particles) is about 1000 MPa.

4.2 Effect of loading rate on the local cleavage fracture stress

The effects of loading rate on σ_f have not been completely validated. In previous works (Chen et al. 1990a, b), σ_f values estimated from Charpy V impact test are essentially the same as that measured by 4PB specimens tested at quasi-static loading, thus it is considered that the σ_f is nearly independent of loading rate. In a recent work (Wang et al. 2004a), 4PB tests of notched specimens loaded at various loading rates for low alloy steels with different grain sizes were done, and the FEM calculations were carried out. It was found that the measured σ_f values do not change with loading rate, as long as the critical event of cleavage fracture does not change. The steels with fine ferrite grains have higher σ_f values and notch toughness, and the critical event of cleavage fracture is the propagation of a ferrite grain-sized crack.

In this work, the σ_f values are accurately measured for a C–Mn steel by 4PB and 3PB tests and combining the FEM calculation of stress distribution ahead of notches at various loading rates. The result in Fig. 14a shows that the local cleavage fracture stress σ_f does not essentially change with loading rate V for the 4PB specimens, and has a large scatter for this steel. According to the works in Ref. (Curry and Knott 1978; Chen et al. 1997b), the σ_f is mainly determined by the critical event of the cleavage fracture. The analysis in Sect. 4.1 shows that for the 4PB specimens of the C–Mn steel, two critical events of crack propagation ($X_f = 0$) and crack nucleation ($X_f \neq 0$) compete in the high stress and strain volume ahead of notch roots at different loading rates tested. While the loading rate varies, the two critical events do not change, that is, the two cleavage micromechanisms do not change. This can be considered as the microscopic reason for the independence of the σ_f on loading rate in the 4PB specimens. For the 3PB specimens, Fig. 14b also shows that the local cleavage fracture stress σ_f does not essentially change with loading rate V. Results of microscopic observation for 3PB tests (Tables 5 and 6, Figs. 12 and 13) are very similar to that for the 4PB tests. So it can be deduced that the characteristics of critical events in the 3PB specimens are the same as that in the 4PB specimens, and it also does not change with the loading rate. This is the reason for the independence of the σ_f on loading rate in the 3PB specimens.

4.3 Effect of notch geometry on the local cleavage fracture stress

Tetelman et al. (1968) investigated the effect of notch root radius on the local cleavage fracture stress σ_f by means of slip-line field analysis. They suggested that when the root radius was larger than 0.254 mm, σ_f may vary with root radius, because of differences in stressed volumes. The work of Lewandowski and Thompson 1986 shows that the σ_f of fully pearlitic microstructure was independent of notch root radius. Yan et al. 1993 evaluated the effect of the notch root radius on σ_f by using FEM analysis and 4PB tests for fine-grain and coarse-grain C–Mn steel. For both fine grains and coarse grains, when the notch root radius increased from 0.25 mm to 1 mm, the stressed volume and fracture load showed marked variations, but σ_f remained relatively constant. Cleavage fracture was related to the elevation of normal stress ahead of the notch and σ_f was independent of the notch root radius. One of the authors of this paper (Wang et al. 1999) investigated the effect of notch depth and notch flank angle on σ_f using FEM analysis and 4PB tests. With increasing notch depths and notch flank angle, the fracture load and "high stress volume" showed marked variation, but σ_f remained relatively constant. The cleavage fracture was related to the elevation of normal stress ahead of the notch and was controlled by the criterion $\sigma_{yy} \geq \sigma_f$. The critical event for cleavage fracture is the propagation of a ferrite grain-sized crack into the neighboring matrix and was independent of the notch depth and flank angle. σ_f was determined by ferrite grain size with a statistical variation. In this work, Fig. 14 show the 4PB and 3PB specimens with two notch geometries have the same σ_f values at various loading rates. This means that the notch geometry has no effects on the σ_f under different

loading rates. The reason for this is also that the critical events in the specimens with different notch geometries do not change.

4.4 Effects of loading mode on the local cleavage fracture stress

The local cleavage fracture stress σ_f is commonly measured by loading notched specimens in 4PB mode (Ritchie et al. 1973, Lewandowski and Thompson 1986; Samant and Lewandowski 1997; Wang et al. 1999, 2003). In this loading mode, the notch was purely bent and only the maximum tensile stress for controlling the cleavage fracture was produced on the notch plane, thus the measurement of the σ_f may be accurate. But when a notched specimen is loaded in 3PB mode, there is a shear force near the notch plane. This may influence the measuring results of the σ_f. So the case that the σ_f was measured by loading notched specimens in 3PB mode can not almost be found in literature. In present work, we measured the σ_f by loading notched specimens in two loading modes (both the 4PB and the 3PB). The results in Fig. 14 show that the measured σ_f values by the two loading modes are almost the same. This means that the shear farce in the 3PB specimens has almost no effect on the measuring results of the σ_f, and the σ_f can be measured by the simple 3PB tests. The data in Tables 3/4 and 5/6 show that the fracture load P_f of the 4PB specimens is larger than that of the 3PB specimens, but the load ratio P_f/P_{gy} at fracture for the two specimens with the same notch geometry is almost the same. The maximum normal stress distributions ahead of the notches of the 4PB and 3PB specimens with the same notch geometry are almost the same (Figs. 4–7). These show that the maximum normal stress distributions ahead of the notches at fracture are almost the same for the 4PB and 3PB specimens with the same notch geometry loaded in the two loading modes. This further indicates that the cleavage fracture is mainly controlled by the maximum normal stress, and the loading mode has no effects on the σ_f. Therefore, the σ_f can be measured by both 4PB and 3PB tests.

4.5 The scatter of the local cleavage fracture stress

According to Curry and Knott 1978, the σ_f can be related to the length C_0 of a microcrack and to the effective surface energy γ by

$$\sigma_f = [2E\gamma/\pi(1-\nu^2)C_0]^{1/2} \quad (1)$$

where E is Young's modulus, and ν is Poisson's ratio. Usually the length C_0 is related to the size of relevant microstructural features. In previous studies on notched specimens ($\rho = 0.25 - 1$ mm, $a = 4.25$ mm, $\theta = 45°$) of C–Mn steels (Yan et al. 1993; Wang et al. 1999), many remaining microcracks were present within the ferrite grains. According to Eq. 1, the σ_f is mainly determined by the sizes of the ferrite grains. The size distribution of ferrite grains causes the scatter of the measured σ_f.

In the present study, the another reason for the larger scatter of σ_f in Fig. 14 is the different critical events in different specimens. When a notched specimen is loaded, a high stress and strain area will be established ahead of the notch root. With increasing the applied load P/P_{gy}, the stress and strain ahead of the notch root are increased, and a weakest constituent (ferrite grain or pearlite colony with a large size and large second phase particles (Chen et al. 1990a; Wang et al. 2004b)) may be sampled at the notch tip and a microcrack may be nucleated at the notch tip due to the highest plastic strain there. If the normal stress σ_{yy} at the notch tip reaches the critical fracture stress σ_f to propagate the just nucleated crack ($\sigma_{yy} \geq \sigma_f$), cleavage fracture occurs. In this case, the critical events are crack propagation, and the cleavages are initiated at the notch tip ($X_f = 0$). The measured σ_f values marked by the solid symbols in Fig. 14 are in a lower scatter range of 1000–1250 MPa, and this lower boundary σ_f value represents the real local cleavage fracture stress of the steel, and it is mainly determined by the size of the ferrite grain (the microcrack length). The corresponding notch toughness characterized by the P_f/P_{gy} data in Tables 3–6 will be low. If a weakest constituent could not be found at the notch tip, with increasing the applied load P/P_{gy} the stress and strain ahead of notch root are further increased. The high normal tensile stress ahead of the notch root may exceed the real critical local fracture stress σ_f, be able to propagate a crack with critical size, but the plastic strain may not have reached a critical value for initiating a crack nucleus. Therefore, in order to produce fracture the load needs to be further increased to increase the plastic strain. When the plastic strain ε_p is increased to a critical value ε_{pc} for initiating a crack nucleus ($\varepsilon_p \geq \varepsilon_{pc}$), fracture occurs. In this case, the critical events are crack nucleation, and the cleavages are initiated at a distance from the notch root

($X_f \neq 0$). The measured σ_f values marked by the open symbols in Fig. 14 are in a higher scatter range of 1250–1500 MPa, and they are the normal stress at the cleavage initiation sites. The corresponding notch toughness characterized by the P_f/P_{gy} data in Tables 3–6 will be high. In essence, the size distribution of the weakest constituent (ferrite grain or pearlite colony with large sizes and large second phase particles) causes the scatter of the measured σ_f and notch toughness of the steel (Chen et al. 1990a, 1997a).

From the discussions above, it could be found that the local cleavage fracture stress σ_f is closely related to the cleavage fracture mechanism (critical events). The σ_f values do not change with loading rate, notch geometry and loading mode, as long as the critical event of cleavage fracture does not change at various testing conditions. The σ_f is mainly determined by the steel microstructure, and it can characterizes intrinsic toughness of steels and may be used in a "local approach" model for assessing integrity of flawed structures.

5 Summary

The local cleavage fracture stress σ_f is regarded as a decisive factor controlling cleavage fracture and toughness of various steels. It is considered to be nearly independent of test temperature, and is taken as a fracture parameter connecting the macroscopic fracture toughness with the steel microstructure. The results in this work combined with previous studies (Wang et al. 1999, 2001, 2003, 2004a, 2004b, 2005) by the authors show that the local cleavage fracture stress σ_f is closely related to the cleavage fracture mechanism (critical events) in steels. The σ_f values do not change with loading rate, notch geometry and loading mode, as long as the critical event of cleavage fracture does not change at various testing conditions. The σ_f is mainly determined by the steel microstructure, and its scatter is mainly caused by the size distribution of the weakest constituent in steels (ferrite grain or pearlite colony with large sizes and large second phase particles) and the change of the critical events in cleavage process. The σ_f can characterize the intrinsic toughness of steels and may be used in a "local approach" model for assessing integrity of flawed structures. The σ_f values could be measured by both 4PB and 3PB tests.

Acknowledgements This work was financially supported by the State Key Laboratory of Advanced Non-Ferrous Metal Materials in Lanzhou University of Technology, and the National Natural Science Foundation of China.

References

Alexander DJ, Lewandowski JJ, Sisak WJ, Thompson AW (1986) Yielding and work hardening effects in notched bend bars. J Mech Phys Solids 34:433–454

Beremin FM (1983) A local criterion for cleavage fracture of a nuclear pressure vessel steel. Metall Trans 14A:2277–2287

Chen JH, Zhu L, Ma H (1990a) On the scattering of the local fracture stress. Acta Metall Mater 38:2527–2535

Chen JH, Wang GZ, Ma H (1990b) Fracture behavior of C–Mn steel and weld metal in notched and precracked specimens, Part II Micromechanism of fracture. Metall Trans 21A:321–330

Chen JH, Wang GZ, Wang Z, Zhu L, Gao YY (1991) Further study on the scattering of local fracture stress and allied toughness values. Metall Trans 22A:2287–2296

Chen JH, Yan C (1992) A comparison of toughness of C–Mn weld steel with different grain sizes. Metall Trans 23A:2549–2556

Chen JH, Hu XJ, Wang GZ (1996) The local fracture stress as a fracture toughness parameter to characterize an heterogeneous weld zone. Fatigue Fract Eng Mater Struct 19:68–80

Chen JH, Wang GZ, Yan C, Ma H, Zhu L (1997a) Advances in the mechanism of cleavage fracture of low alloy steel at low temperature Part III: local fracture stress σ_f. Int J Fract 83:139–157

Chen JH, Wang GZ, Yan C, Ma H, Zhu L (1997b) Advances in the mechanism of cleavage fracture of low alloy steel at low temperature. Part I: Critical event. Int J Fract 83:105–120

Curry DA (1980) Cleavage micromechanisms of crack extension in steel. Metal Sci August–September:319–326

Curry DA, Knott JF (1978) Effect of microstructure on cleavage fracture stress in steel. Mater Sci Nov:511–514

Gao X, Dodds RH Jr, Tregoning RL, Joyce JA (2001) Weibull stress model for cleavage fracture under high-rate loading. Fatig Fract Eng Mater Struct 24:551–564

Griffith JR, Owen DRJ (1971) An elastic-plastic stress analysis for a notched bar in plane strain bending. J Mech Phys Solids 19:419–431

Hahn GT (1984) The influence of microstructure on brittle fracture toughness. Metall Trans A 15A:947–959

Kavishe FRL, Baker TJ (1986) Micromechanism of cleavage fracture in fully pearlitic steels. Mater Sci Technol 2:583–588

Knott JF (1966) Some effects of hydrostatic tension on the fracture behavior of mild steel. J Iron Steel Inst 204:104–111

Lewandowski JJ, Thompson AW (1986) Microstructural effects on the cleavage fracture stress of fully pearlitic eutectoid steel. Metall Trans 17A:1769–1786

Lin T, Evans AG, Ritchie RO (1986) A statistical model of brittle fracture by transgranular cleavage. J Mech Phys Solids 34:477–497

Mendiratta MG, Goetz RL, Dimiduk DM (1996) Notch fracture in γ-titanuim aluminides. Metall Mater Tran 27A:3903–3912

Minami F, Bruckner-Foit A, Munz D, Trolldenier B (1992) Estimation procedure for the Weibull parameters used in the local approach. Int J Fract 54:197–210

Mudry F. (1987) A local approach to cleavage fracture. Nucl Eng Des 105:65–76

Pineau A (2006) Development of the local approach to fracture over the past 25 years: theory and applications Int J Fract 138:139–166

Ritchie RO, Knott JF, Rice JR (1973) On the relationship between critical tensile stress and fracture toughness in mild steel. J Mech Phys Solids 21:395–410

Ritchie RO, Francis B, Server WL (1976) Evaluation of toughness in ALSL 4340 alloy steel austenitized at low and high temperatures. Metall Trans 7A:831–838

Ritchie RO, Server WL, Wullaert RA (1979) Critical fracture stress and fracture strain models for the prediction of lower and upper shelf toughness in nuclear pressure vessel steels. Metall Trans 10A:1557–1570

Ritchie RO, Thompson AW (1985) On macroscopic and microscopic analyses for crack initiation and crack growth toughness in ductile alloys. Metall Trans 16A:233–248

Ruggieeri C, Dodds RH (1996) A transferability model for brittle fracture including constraint and ductile tearing effects: a probabilistic approach. Int J Fract 79:309–340

Samant AV, Lewandowski JJ (1997) Effects of test temperature, grain size, and alloy additions on the cleavage fracture stress of polycrystalline niobium. Metall Mater Trans 28A:389–399

Tetelman AS, Wilshaw TR, Rau CA Jr (1968) The critical tensile stress criterion for cleavage. Int J Fract 4:147–157

Thompson AW, Knott JF (1993) Micromechanisms of brittle fracture. Metall Trans A 24A:523–534

Wall M, Lane CE, Hippsley CA (1994) Fracture criteria for hydrogen and temper embrittlement in 9Cr1Mo steel. Acta Metall Mater 42:1295–1309

Wallin K (1984) The scatter in K_{1c} results. Eng Fract Mech 19:1085–1093

Wang GZ, Chen JH (1998) Cleavage fracture criterion of low alloy steel and weld metal in notched specimens. Int J Fract 89:269–284

Wang GZ, Wang HJ, Chen JH (1999) Effects of notch geometry on the local cleavage fracture stress σ_f. Fatigue Fract Eng Mater Struct 22:849–858

Wang GZ, Liu GH, Chen JH (2001) Effects of precracked specimen geometry on local cleavage fracture stress σ_f of low alloy steel. Int J Fract 112:183–196

Wang GZ, Wang JG, Chen JH (2003) Effects of geometry of notched specimens on the local cleavage fracture stress σ_f of C–Mn steel. Eng Fract Mech 70:2499–2512

Wang GZ, Ren XC, Chen JH (2004a) Effects of loading rate on fracture behavior of low-alloy steel with different grain sizes. Metall Mater Trans A 35A:1765–1778

Wang GZ, Liu YG, Chen JH (2004b) Investigation of cleavage fracture initiation in notched specimen of a C–Mn steel with carbides and inclusions. Mater Sci Eng A 369:181–191

Wang GZ, Wang YL, Chen JH (2005) Effects of loading rate on the local cleavage fracture stress σ_f in notched specimens. Eng Fract Mech 72:675–689

Yan C, Chen JH, Sun J, Wang Z (1993) Critical assessment of the local cleavage stress in notched specimens of C–Mn steel. Metall Trans 24A:1381–1389